

Research Article

Pixel Intensity Clustering Algorithm for Multilevel Image Segmentation

Oludayo O. Olugbara, Emmanuel Adetiba, and Stanley A. Oyewole

ICT and Society Research Group, Durban University of Technology, P.O. Box 1334, Durban 4000, South Africa

Correspondence should be addressed to Oludayo O. Olugbara; oludayoo@dut.ac.za

Received 20 May 2015; Accepted 12 July 2015

Academic Editor: María I. Herreros

Copyright © 2015 Oludayo O. Olugbara et al. This is an open access article distributed under the Creative Commons Attribution License, which permits unrestricted use, distribution, and reproduction in any medium, provided the original work is properly cited.

Image segmentation is an important problem that has received significant attention in the literature. Over the last few decades, a lot of algorithms were developed to solve image segmentation problem; prominent amongst these are the thresholding algorithms. However, the computational time complexity of thresholding exponentially increases with increasing number of desired thresholds. A wealth of alternative algorithms, notably those based on particle swarm optimization and evolutionary metaheuristics, were proposed to tackle the intrinsic challenges of thresholding. In codicil, clustering based algorithms were developed as multidimensional extensions of thresholding. While these algorithms have demonstrated successful results for fewer thresholds, their computational costs for a large number of thresholds are still a limiting factor. We propose a new clustering algorithm based on linear partitioning of the pixel intensity set and between-cluster variance criterion function for multilevel image segmentation. The results of testing the proposed algorithm on real images from Berkeley Segmentation Dataset and Benchmark show that the algorithm is comparable with state-of-the-art multilevel segmentation algorithms and consistently produces high quality results. The attractive properties of the algorithm are its simplicity, generalization to a large number of clusters, and computational cost effectiveness.

1. Introduction

Image segmentation remains an important problem in the fields of digital image processing, pattern analysis, image understanding, and computer vision. It is the process of subdivision of an image into homogeneous and disjoint sets sharing similar properties such as intensity, color, and contour [1]. Applications of image segmentation cut across disciplines as diverse as pattern recognition, image compression, content-based image retrieval, image processing, microscopic imaging, automatic image analysis, image and video understanding, video security, computer-aided surgery, automated medical diagnosis, human-machine interface, moving object tracking, image enhancement, biometric access control, computer vision, deoxyribonucleic acid sequencing, automatic vehicle recognition, optical character recognition, remote sensing, land cover classification, and machine learning [2–10]. Image segmentation is not a trivial problem because the majority of images are affected by factors such

as noise content, occlusion, weak object boundary, inhomogeneous object region, weak contrast, nonuniformity of illumination, and reflectance [4, 11]. Different algorithms have been proposed over the years for image segmentation and two important properties commonly employed to categorize various segmentation algorithms are homogeneity and discontinuity of pixel properties. Edge-based methods are based on pixel discontinuity properties and they segment images by detecting pixels with rapid transition in intensities between regions [12, 13]. The image segmentation methods based on the property of homogeneity include thresholding, clustering, and region growing as well as region splitting and merging [14, 15]. These methods segment images based on the predefined objective functions and characteristics such as texture, shape, color, intensity, and other domain specific features [11, 16].

Image thresholding is very popular because it offers intrinsic benefits such as compact storage space, fast execution speed, simplicity, low computational cost, and real-time

applicability [17, 18]. Thresholding attempts to identify and extract an object from its background on the basis of the distribution of gray levels or texture in the image object [19]. The prime objective of gray level image thresholding is to divide a gray level image into a K -number of predetermined partitions or clusters based on $K - 1$ different thresholds [20]. Image thresholding can be appositely classified into parametric and nonparametric methods. In parametric approach, a statistical model and a histogram are employed to obtain a set of parameters that control the fitness of the model. In the nonparametric approach, thresholds are chosen through the optimization of certain objective functions such as between-cluster variance, within-cluster variance, two-dimensional entropy, and cross entropy [21, 22]. Nonparametric thresholding can be realized either globally or locally. In the global implementation, object and background pixels are discriminated by comparing them with a chosen threshold and binary partitioning is used to segment the image. On the other hand, local thresholding finds a local threshold by examining the intensity values of the local neighborhood of each pixel. The Otsu algorithm [21] is one of the most widely used for global nonparametric thresholding. It provides a threshold by maximizing the between-cluster variance in the histogram of a gray level image. The algorithm is not complicated because it assumes the image histogram to be bimodal, meaning that there are two clusters or one threshold. However, bimodal thresholding cannot always achieve satisfactory results when the histogram of the image gray level is nonbimodal [20, 23]. Despite the position of Otsu that extending his algorithm to multilevel thresholding is a straightforward problem, he affirmed that “the selected thresholds become less credible as the number of levels increases” [21]. This is because the choice of appropriate thresholds is germane; making this choice manually or automatically is often complicated and several iterations are required to compute the zeroth and the first-order moments of multiple clusters [24].

Clustering techniques were described in [25] as multi-dimensional extensions of thresholding concepts and they are reputed in the literature to be very popular for image segmentation [26]. Clustering is an unsupervised learning task in which a finite set of clusters is identified so as to classify the pixels in a digital image. In clustering, the number of clusters is known a priori and image pixels are grouped into appropriate clusters based on the principle of intracluster similarity maximization or intercluster similarity minimization [27]. Clustering based segmentation algorithms can be divided into two broad categories, which are hard clustering and soft clustering. Hard clustering methods are used for datasets with sharp boundaries between clusters and a pixel belongs to only one cluster. K -means clustering is one of the most prevalent hard clustering algorithms because of its implementation simplicity and low computational costs [28]. The conventional K -means algorithm assigns each pixel in an image to the respective clusters on the basis of the minimum Euclidean distance. Meanwhile, one of the shortcomings of this algorithm is that poor assignment of pixels often occurs in situations where the pixel has the same minimum Euclidean distance to two or more clusters. An improper initialization procedure also gets the cluster centers in the

conventional K -means algorithm trapped in local minimal or stuck to the initial values so that they are unable to represent any group of data effectively. These scenarios often result in some clusters becoming dead centers, a situation in which clusters have no members [29].

In this study, we develop a new multilevel image segmentation method named Pixel Intensity Clustering Algorithm (PICA). Firstly, we utilized the set of image pixel intensities, the number of desired clusters, and a linear partitioning scheme to perform the initialization of cluster centroids. This initialization strategy is a notable departure from the use of randomization to determine initial cluster centroids, which is the custom in conventional clustering based segmentation algorithms. Our initialization scheme fulfills an important purpose of eliminating the incidence of dead centers, which is a common problem in conventional clustering based image segmentation algorithms [29]. Secondly, we adopted Otsu's between-cluster variance criterion function [21] frequently used in multilevel thresholding to place pixel intensities into suitable clusters. Thirdly, in order to obtain the segmented image output, the input image is reconfigured based on the outcome of the clustering procedures in the preceding steps. The reconfiguration process uses the input image as a reference to generate the segmented image; the pixel intensity at each spatial location in the output image is assigned the centroid of the cluster to which the pixel intensity in the input image belongs. The number of pixel intensities in an input image histogram is generally far smaller than the size of the image; therefore, the use of pixel intensities of the image histogram (here called pixel intensity set) both for centroid initialization and for pixel clustering is a strong strategy for the computational cost reduction in PICA. The use of this approach obviously implies that the time complexity of PICA is proportionate to the size of the input image. PICA does not utilize spatial information as widely suggested [30], yet it achieves remarkable performance in segmentation result and computational time. Moreover, PICA satisfies survivability and recoverability principles because it can work for any number of clusters from 2 up to the maximum number of pixel intensities in the input image without breaking down. It also satisfies the principle of simplicity because it does not have to perform complex mathematical operations to achieve the desired result.

2. Relevant Literature

In recent years, a number of improved Otsu algorithms for multilevel thresholding were credited with the capability to reduce computational inefficiency. For instance, a Two-Stage Multithreshold Otsu (TSMO) algorithm was developed to improve the performance of the original Otsu algorithm [31]. The principle employed in TSMO for finding multilevel thresholds of an image is similar to that of the original Otsu method. It utilizes the statistical groups M_z (16, 32, 64) with each group containing N_z ($=256/M_z$) gray levels to determine thresholds in two stages by applying Otsu criterion twice. Low classification errors were reported in the application of TSMO for test images with five thresholds. However, as reported, the TSMO algorithm cannot always

guarantee a satisfactory performance for many complex images. The TSMO algorithm was later extended by Huang et al. [23], wherein they used the valley estimation scheme for automatic cluster determination. The experimental results of their study showed that the speed of computation is about 19000 times faster than the original Otsu algorithm when the number of clusters is seven. However, real-time performance was achieved when the number of clusters is fewer than six or five thresholds.

Besides the TSMO algorithm and its extensions, other algorithms have utilized different objective functions for multilevel thresholding. For example, Dong et al. [18] developed a linear iterative algorithm to determine thresholds that minimize a weighted sum-of-squared error objective function. The technique employed is mathematically tantamount to the Otsu algorithm, but 200 times faster in computational time. The algorithm may predictably not produce satisfactory results in large clusters because it was not extended to segment images beyond three clusters. Metaheuristic methods, such as Genetic Algorithm (GA), Artificial Bee Colony (ABC), Differential Evolution (DE), electromagnetism optimization (EMO), Bat Algorithm (BA), particle swarm optimization (PSO), Darwinian PSO (DPSO), and Fractional-Order DPSO (FODPSO) [1, 7, 17, 32–36], have also been applied for multilevel thresholding. One of the best algorithms known amongst these metaheuristic algorithms is the PSO. It was illustrated in [37] that the PSO-based segmentation method acted better than other metaheuristic methods in terms of precision, robustness of results, and runtime. Nevertheless, a general problem with the PSO and similar optimization methods is that they may be trapped in local optimum points which consequently imply that the algorithm may work for some problems but may fail in others. DPSO and FODPSO were later proposed to solve this problem and it was proved that the FODPSO is faster than the PSO and more efficient than the DPSO [38, 39]. However, since all metaheuristic algorithms are random and stochastic, the outputs of FODPSO algorithm are not always the same in each run and, for large data, the efficiency of the method is constrained to a great extent [36].

There are several improvements of the conventional K -means algorithm in the literature, which include moving K -means (MKM), adaptive moving K -means (AMKM), adaptive fuzzy moving K -means (AFMKM), and enhanced moving K -means (EMKM) [29, 40, 41]. The MKM, AMKM, and AFMKM methods homogeneously segment images, but they are still extremely sensitive to the poor initialization problem which is the major defect of clustering based segmentation methods. The EMKM, which is an improved version of AMKM, is nevertheless less sensitive to the initialization problem. However, the literature is replete with the fact that MKM, AMKM, AFMKM, and even EMKM cannot satisfactorily differentiate between dead centers and clusters with zero intracluster variance. Consequently, these methods fail to adequately distribute the pixels in an image into the appropriate clusters [29]. Soft clustering was later introduced to solve some of the inherent problems in hard clustering methods. Soft clustering algorithms are used when there are no hard boundaries amongst objects in an image and they

introduce fuzziness by partly allocating pixels to all clusters with different degrees of membership. Examples of soft clustering methods are fuzzy C -means (FCM), Gustafson-Kessel, Gaussian mixture decomposition, and fuzzy C -varieties, but one of the most popular of all is the FCM algorithm [28, 29]. When compared with its hard clustering counterpart, conventional FCM is able to preserve more information from the original image. Nevertheless, the conventional FCM algorithm does not consider spatial information in the original image and because of this negligence, the algorithm is very sensitive to noise and outliers in the image. This shortcoming has led to the development of several other algorithms [42] that incorporated spatial information to enhance the conventional FCM algorithm. It is however reported in the literature that the computational time of many of these enhanced FCM algorithms is dependent on the size of the image and, therefore, the larger the image size, the more the segmentation time [42].

The foregoing review of existing studies generally shows that both thresholding and clustering based multilevel image segmentation algorithms in the literature are laden with research gaps [6, 26]. These gaps served as a strong motivation for this study.

3. Methodology

3.1. Proposed Algorithm. There are three main steps involved in PICA, initialization of cluster centroids, allocation of pixel intensities into clusters, and computation of output image. PICA fulfills the essential properties of clustering, which implies that, given an $M \times N$ input image, the algorithm finds K clusters $C = (c_0, c_1, \dots, c_{K-1})$ such that the similarity of the pixel intensities in the same cluster c_j , $j = 0, 1, \dots, K - 1$, is high while pixel intensities from different clusters are highly dissimilar and the clusters fulfill the following desirable properties [43]:

- (a) $C_j \neq \{\}$, $\forall j = 0, 1, \dots, K - 1$; every cluster has at least one pixel intensity and there is no dead center syndrome.
- (b) $C_i \cap C_j \neq \{\}$, $\forall i, j = 0, 1, \dots, K - 1$; a pixel intensity cannot belong to more than one cluster.

The formulation of PICA proceeds as follows, assuming inputs to the algorithm are 2-dimensional grayscale image and the number of desired clusters is specified.

Step 1 (initialization of cluster centroids). The initialization of cluster centroids begins with the estimate of cluster weight. Cluster weight is the cumulative probabilities of pixel intensities in a cluster. If the input image is represented in L pixel intensities $(0, 1, 2, \dots, L - 1)$, the number of pixels at intensity level i is denoted by f_i and the total number of pixels equals $f = f_0 + f_1 + \dots + f_{L-1}$. The occurrence probability $p(i)$ for a given pixel intensity i is given by

$$p(i) = \frac{f_i}{f}, \quad p(i) \geq 0, \quad \sum_{i=0}^{L-1} p(i) = 1. \quad (1)$$

The linear partitioning of a set of image pixel intensities is a useful strategy to guess the initial cluster centroids. Let $S = \{e_0, e_1, \dots, e_{Q-1}\}$, $Q \leq L$, be the set of image pixel intensities such that for every element $e_t \in S$ the condition $p(e_t) > 0$ is satisfied. The purpose of the linear partitioning strategy is to guess the initial K cluster centroids from the set S . This set partitioning strategy provides a mechanism to avoid the incidence of dead centers when guessing the initial cluster centroids. The dead center syndrome is a common problem often associated with clustering methods [30, 43–45]. In codicil, the set partitioning strategy provides an easy generalization of our algorithm to the case of Q number of clusters with lower computational costs. The generalization of multilevel image segmentation portrays the recoverability property of our algorithm. The set partitioning strategy of PICA replaces the random selection strategy, which is the usual practice in the conventional clustering algorithms [29].

Supposing the pixel intensity $e_t \in S$ is to be selected as the initial centroid of the cluster j , $j = 0, 1, 2, \dots, K - 1$, the weight of this cluster can be estimated as follows:

$$w_j = p(e_t). \quad (2)$$

The variable j is interpreted in this work as the cluster label, which is a number that associates a given image pixel intensity with its cluster. This implies that two or more image pixel intensities belonging to the same cluster would have the same cluster label for the purpose of easy grouping. The index t of the pixel intensity $e_t \in S$ is obtained as follows:

$$t = (\text{int})\left(\frac{j * Q}{K}\right), \quad Q, K = 2, 3, \dots, L. \quad (3)$$

The cluster centroid (μ_j), which is widely known as the center of gravity or center of mass of the j th cluster, is defined as

$$\mu_j = \frac{w'_j}{w_j}. \quad (4)$$

The parameter w'_j is defined as follows:

$$w'_j = e_t * p(e_t). \quad (5)$$

Step 2 (allocation of pixel intensities into clusters). The remaining $Q - K$ number of image pixel intensities in S not already allocated in clusters in Step 1 has to be allocated to suitable clusters based on the maximization of between-cluster variance. The cluster labels are then assigned to the allocated image pixel intensities and cluster centroids are updated accordingly. The maximization of the generalized between-cluster variance in allocating pixel intensities to suitable clusters, as used in PICA, is a departure from the minimization of Euclidean distance objective function that has hitherto been the norm in the clustering based image segmentation methods. In conventional clustering based image segmentation methods, cases in which a pixel has the same minimum Euclidean distance to two or more clusters have been reported to result in poor allocation of pixel

intensities, which consequently lead to poor segmentation result [29, 46]. The between-cluster variance is defined as the sum of weighted squared distances (variances) between cluster centroids and grand or global centroid [22]:

$$\max \left\{ \sigma_B^2 = \sum_{j=0}^{K-1} w_j (\mu_j - \mu_g)^2 \right\}, \quad (6)$$

where the parameter μ_g is the global centroid of the image pixel intensities and it can be estimated as

$$\mu_g = \sum_{i=0}^{L-1} i p_i. \quad (7)$$

If $i(x, y)$ is the pixel intensity at the spatial location (x, y) in $M \times N$ (M is the height and N is the width) of the input image, the global centroid can also be estimated directly from the image data, instead of from the image histogram as follows:

$$\mu_g = \frac{1}{M * N} \sum_{x=0}^{M-1} \sum_{y=0}^{N-1} l(x, y). \quad (8)$$

The weight and centroid of the cluster that the pixel intensity e_i , $i = K, K + 1, \dots, Q - 1$, is allocated to have to be updated according to the following update rules:

$$\begin{aligned} w_j &= w_j + p(e_i), \\ w'_j &= w'_j + e_i * p(e_i), \\ \mu_j &= \frac{w'_j}{w_j}. \end{aligned} \quad (9)$$

This update mechanism ensures that the weights of all clusters add up to unity, following the probability theory; that is,

$$\sum_{j=0}^{K-1} w_j = 1. \quad (10)$$

Step 3 (computation of output image). The output image is generated by assigning to the pixel intensity at the spatial location (x, y) in the output image the cluster centroid of the corresponding pixel intensity at the spatial location (x, y) in the input image. Given a pixel intensity at location (x, y) from an input image, the cluster label of this pixel intensity has to be determined. Using this cluster label, the centroid of the cluster that this pixel was allocated to can be determined. The implementation of PICA could be compactly outlined based on the above description as in Algorithm 1.

3.2. Estimated Time Complexity. The analysis of time complexity of PICA can be performed for each step of the algorithm. In Step 1, the number of instructions can be executed in $O(MN)$, which is linear with respect to the number of pixel $M \times N$ in the input image. The total number of instructions executed in Step 1 is the number of instructions to create an image histogram, compute probabilities of pixel intensities,

Input: $M \times N$ grayscale image, K number of clusters.

Output: $M \times N$ grayscale image.

Let $S = (e_0, e_1, \dots, e_{Q-1})$, $Q \leq L$ represents the set of image pixel intensities and assuming BCV is the between cluster variance.

```

(1) for all  $j = 0, 1, \dots, K - 1$  do
(2)    $t = (\text{int})((j * Q)/K)$ 
(3)   estimate the  $j$ th cluster centroid using the pixel intensity  $e_t$ 
(4)   assign cluster label  $j$  to the pixel intensity  $e_t$ 
(5)   swap the pixel intensity  $e_t$  with the pixel intensity  $e_j$ 
(6) end for
(7) for all  $i = K, K + 1, \dots, Q - 1$  do
(8)   for all  $j = 0, 1, \dots, K - 1$  do
(9)     tentatively allocate pixel intensity  $e_i$  to the  $j$ th cluster
(10)     $BCV = w_j * (\text{variance of the } j\text{th cluster centroid})$ 
(11)    for all  $k = 0, 1, \dots, K - 1$  and  $j$  not equal to  $k$  do
(12)       $BCV = BCV + w_k * (\text{variance of the } k\text{th cluster centroid})$ 
(13)    end for
(14)  end for
(15)  permanently allocate  $e_i$  to the cluster that gives maximum BCV
(16)  assign cluster label to the allocated pixel intensity  $e_i$ 
(17)  update cluster centroid
(18) end for
(19) compute output image
(20) stop

```

ALGORITHM 1: PICA of $O(MN + QK^2)$.

determine set of image pixel intensities, compute global centroid, estimate initial cluster weight, determine initial cluster centroids, assign cluster labels to pixel intensities, and swap pixel intensities. All of these instructions can be executed in time complexity of $O(M \times N)$, provided $M \times N \gg L$. The number of instructions required to compute the output image in Step 3 also can be executed in $O(MN)$. The instructions in Step 2 are only executed whenever $K \neq Q$ and they can be executed in $O(QK^2 - K^3) < O(QK^2)$. The time complexity of PICA can therefore be approximated by $O(MN + QK^2)$.

The computational time complexity of PICA is compared to that of conventional K -means algorithm and optimized K -means algorithm to strengthen the illustration of the computational speed advantage of the algorithm. We decided to select these algorithms because the conventional K -means algorithm was proven to have a shorter processing time with complexity of $O(ndkt)$ and also the optimized K -means algorithm was reputed to have time complexity of $O(ndktb)$ [29, 47]. These parameters, n (which corresponds to MN), d , k (which corresponds to K), t , and b , are, respectively, the number of pixels in an input image, the number of attribute dimensions, the number of clusters, the number of iterations, and the number of intensity values of the conflict pixels to be assigned to their respective clusters. PICA outperforms these algorithms in computational time complexity as parameter values become large. In fact, practical experience shows that KM, PSO, DPSO, and FDPSO took longer time to process and broke down when $K > 180$ on the selected images from Berkeley Segmentation Dataset and Benchmark.

4. Experiments and Results

The experimental setup for this study and the numerical results obtained for the proposed algorithm are reported. Furthermore, empirical results of segmentation using the proposed algorithm were compared both qualitatively and quantitatively with state-of-the-art algorithms. The following subsections contain details of the experimental setup, the numerical results, and the comparative results.

4.1. Experimental Setup. All the experiments in this study were performed on an Intel Core i7 processor @ 3.5 GHz with 64 GB of RAM running the Windows XP operating system. The algorithm was implemented in C/C++. The program is very compact, well-structured, and easy to follow, which is one of the bases of the intrinsic simplicity of the algorithm. The input image to the program was in grayscale, but the program can as well process color images by processing each RGB channel separately and then combine the results. The ITU-R recommendation (ITU-R BT.709-5) was applied to convert a color image to a grayscale image before the program was executed. We collected twelve images from the Berkeley Segmentation Dataset and Benchmark with identification numbers "45077," "157055," "78098," "42049," "253027," "169012," "210088," "208001," "10081," "155060," "25098," and "35070" [48].

4.2. Numerical Results. In this section, we report the results of the computations carried out by the proposed algorithm to determine some salient parameters, which are initial cluster

TABLE 1: Initial cluster centroids.

Image	Cluster	Initial cluster centroids	
45077	3	9, 89, 169	
	4	9, 69, 129, 189	
	5	9, 57, 105, 153, 201	
	6	9, 49, 89, 129, 169, 209	
	7	9, 43, 77, 111, 146, 180, 214	
	8	9, 39, 69, 98, 129, 159, 189, 219	
	9	9, 35, 62, 89, 114, 142, 169, 195, 222	
	10	9, 33, 57, 81, 105, 129, 153, 177, 201, 225	
	11	9, 30, 52, 74, 96, 118, 139, 161, 183, 205, 227	
	12	9, 29, 49, 69, 89, 109, 129, 149, 169, 189, 209, 229	
	157055	3	31, 106, 180
		4	31, 87, 143, 199
5		31, 76, 120, 165, 210	
6		31, 69, 106, 143, 180, 217	
7		31, 63, 95, 127, 159, 191, 223	
8		31, 59, 87, 115, 143, 171, 199, 227	
9		31, 56, 81, 106, 131, 155, 180, 205, 230	
10		31, 54, 76, 98, 120, 143, 165, 188, 210, 232	
11		31, 52, 72, 92, 113, 133, 153, 173, 193, 214, 233	
12		31, 50, 69, 87, 106, 124, 143, 162, 180, 199, 217, 236	
78098		3	0, 84, 168
		4	0, 63, 126, 189
	5	0, 50, 101, 151, 202	
	6	0, 42, 84, 126, 168, 210	
	7	0, 36, 72, 107, 144, 180, 216	
	8	0, 31, 63, 94, 126, 158, 189, 221	
	9	0, 28, 56, 84, 112, 140, 168, 196, 224	
	10	0, 25, 50, 75, 101, 126, 151, 177, 202, 227	
	11	0, 23, 46, 69, 92, 115, 138, 161, 184, 207, 230	
	12	0, 21, 42, 63, 84, 105, 126, 147, 168, 189, 210, 231	
	42049	3	10, 87, 165
		4	10, 68, 126, 184
5		10, 56, 102, 149, 196	
6		10, 48, 87, 126, 165, 204	
7		10, 42, 76, 109, 143, 176, 209	
8		10, 38, 68, 97, 126, 155, 184, 213	
9		10, 35, 61, 87, 113, 139, 165, 191, 217	
10		10, 33, 56, 79, 102, 126, 149, 173, 196, 219	
11		10, 31, 52, 73, 94, 115, 137, 158, 179, 200, 221	
12		10, 29, 48, 68, 87, 107, 126, 145, 165, 184, 204, 223	
253027		3	32, 107, 181
		4	32, 88, 144, 199
	5	32, 77, 121, 166, 210	
	6	32, 70, 107, 144, 181, 218	
	7	32, 64, 96, 128, 159, 191, 223	
	8	32, 60, 88, 116, 144, 171, 199, 227	
	9	32, 57, 82, 107, 131, 156, 181, 204, 230	
	10	32, 55, 77, 99, 121, 144, 166, 187, 210, 232	
	11	32, 52, 73, 93, 113, 133, 154, 174, 194, 214, 234	
	12	32, 51, 70, 88, 107, 124, 144, 162, 181, 199, 218, 236	

TABLE 1: Continued.

Image	Cluster	Initial cluster centroids	
169012	3	20, 98, 176	
	4	20, 78, 137, 196	
	5	20, 67, 114, 161, 208	
	6	20, 59, 98, 137, 176, 215	
	7	20, 53, 87, 120, 154, 187, 221	
	8	20, 49, 78, 108, 137, 166, 196, 225	
	9	20, 46, 72, 98, 124, 150, 176, 202, 228	
	10	20, 43, 67, 90, 114, 137, 161, 184, 208, 231	
	11	20, 41, 62, 84, 105, 126, 148, 169, 190, 212, 233	
	12	20, 39, 59, 78, 98, 117, 137, 157, 176, 196, 215, 235	
	210088	3	33, 106, 180
		4	33, 88, 143, 198
5		33, 77, 121, 165, 209	
6		33, 69, 106, 143, 180, 217	
7		33, 64, 96, 127, 159, 190, 222	
8		33, 60, 88, 115, 143, 171, 198, 225	
9		33, 57, 82, 106, 131, 155, 180, 204, 229	
10		33, 55, 77, 99, 121, 143, 165, 187, 209, 231	
11		33, 53, 73, 93, 113, 133, 153, 173, 193, 213, 233	
12		33, 51, 69, 88, 106, 125, 143, 161, 180, 198, 217, 234	
208001		3	4, 87, 169
		4	4, 66, 128, 190
	5	4, 54, 103, 153, 202	
	6	4, 46, 87, 128, 169, 209	
	7	4, 40, 75, 110, 146, 181, 216	
	8	4, 35, 66, 97, 128, 159, 190, 221	
	9	4, 32, 58, 87, 114, 142, 169, 197, 224	
	10	4, 29, 54, 79, 103, 128, 153, 177, 202, 226	
	11	4, 27, 49, 72, 94, 117, 139, 162, 184, 207, 229	
	12	4, 25, 46, 66, 87, 107, 128, 149, 169, 190, 209, 231	
	10081	3	5, 89, 172
		4	5, 68, 130, 191
5		5, 55, 105, 155, 205	
6		5, 47, 89, 130, 172, 213	
7		5, 41, 77, 111, 148, 183, 219	
8		5, 37, 68, 99, 130, 161, 191, 223	
9		5, 33, 61, 89, 116, 144, 172, 199, 227	
10		5, 29, 55, 80, 105, 130, 155, 180, 205, 230	
11		5, 28, 51, 73, 96, 119, 141, 164, 187, 209, 232	
12		5, 26, 47, 68, 89, 109, 130, 151, 172, 191, 213, 234	
155060		3	1, 85, 169
		4	1, 64, 127, 190
	5	1, 51, 102, 152, 203	
	6	1, 43, 85, 127, 169, 211	
	7	1, 37, 73, 109, 145, 181, 217	
	8	1, 32, 64, 95, 127, 159, 190, 222	
	9	1, 29, 57, 85, 113, 141, 169, 197, 225	
	10	1, 26, 51, 76, 102, 127, 152, 178, 203, 228	
	11	1, 24, 47, 70, 93, 116, 139, 162, 185, 207, 231	
	12	1, 22, 43, 64, 85, 106, 127, 148, 169, 190, 211, 232	

TABLE 1: Continued.

Image	Cluster	Initial cluster centroids	
35070	3	18, 86, 154	
	4	18, 69, 120, 171	
	5	18, 58, 99, 140, 180	
	6	18, 52, 86, 120, 154, 188	
	7	18, 47, 76, 105, 134, 163, 192	
	8	18, 43, 69, 94, 120, 145, 171, 196	
	9	18, 40, 63, 86, 108, 131, 154, 176, 199	
	10	18, 37, 58, 79, 99, 120, 140, 160, 180, 201	
	11	18, 36, 55, 73, 92, 110, 129, 147, 166, 184, 203	
	12	18, 35, 52, 69, 86, 103, 120, 137, 154, 171, 188, 205	
	25098	3	3, 87, 171
		4	3, 66, 129, 192
5		3, 53, 103, 154, 203	
6		3, 45, 87, 129, 171, 213	
7		3, 39, 75, 111, 147, 183, 219	
8		3, 34, 66, 97, 129, 160, 192, 223	
9		3, 31, 59, 87, 115, 143, 171, 199, 226	
10		3, 28, 53, 78, 103, 129, 154, 179, 203, 229	
11		3, 25, 48, 71, 94, 117, 140, 163, 186, 209, 232	
12		3, 23, 45, 66, 87, 108, 129, 150, 171, 192, 213, 234	

centroids, updated cluster centroids, and cluster weights. The values of these parameters for the twelve images selected from the Berkeley Segmentation Dataset and Benchmark are shown in Tables 1, 2, and 3. In particular, Table 1 shows the initial cluster centroids computed for each of the twelve images from clusters 3 to 12 using (1) to (5). The values that are reported in Table 1 clearly indicate orderly sequences of numbers across the different clusters of many of the test images. This result illustrates the merit of the linear partitioning scheme for the initialization step of PICA. It can also be seen in Table 1 that the more the number of clusters, the better the spread of the initial cluster centroids towards the highest pixel intensity value in the input image. This apparently explains why better segmentation is achieved at a higher number of clusters for the proposed PICA because of the better representation of the pixel intensity in the input image.

Table 2 shows the final updated cluster centroids for clusters 3 to 12 for all the test images used in this study. These values were computed based on (9). The cluster centroid update procedure based on these equations can be deemed successful as reflected in the visual result of the segmentation. For instance, in Table 2, the initial centroids of the image “45077” for four clusters, which were 9, 69, 129, and 189, were updated to the final values of 39, 74, 109, and 159, showing that an update was actually performed. Similar results were obtained for all the other test images used in this study as shown in Table 2. The updated cluster centroids finally computed by the proposed algorithm tend towards the higher pixel intensity value in the input as the number of clusters is increased. This significantly contributes to the enhancement of the segmentation result in higher clusters. These values of

TABLE 2: Final updated cluster centroids.

Image	Cluster	Final updated cluster centroids	
45077	3	46, 87, 143	
	4	39, 74, 109, 159	
	5	34, 64, 97, 162, 127	
	6	32, 54, 91, 117, 160, 73	
	7	30, 48, 72, 109, 136, 173, 92	
	8	28, 44, 67, 99, 121, 147, 180, 83	
	9	26, 40, 62, 82, 112, 134, 157, 185, 98	
	10	25, 37, 58, 78, 105, 124, 145, 166, 189, 92	
	11	23, 35, 52, 70, 97, 111, 132, 152, 187, 169, 84	
	12	23, 34, 49, 65, 89, 105, 123, 141, 168, 188, 155, 77	
	157055	3	55, 114, 192
		4	51, 88, 138, 199
5		49, 74, 119, 165, 211	
6		47, 65, 103, 135, 172, 215	
7		46, 61, 92, 112, 159, 186, 220	
8		45, 59, 84, 112, 137, 166, 193, 223	
9		44, 57, 77, 103, 125, 154, 175, 198, 226	
10		44, 55, 72, 96, 118, 138, 163, 183, 204, 229	
11		43, 54, 68, 89, 110, 127, 151, 169, 189, 207, 231	
12		42, 52, 64, 82, 103, 121, 139, 160, 177, 195, 212, 235	
78098		3	30, 80, 176
		4	23, 64, 113, 200
	5	19, 52, 92, 132, 211	
	6	16, 44, 78, 115, 155, 221	
	7	14, 39, 68, 100, 131, 168, 227	
	8	13, 34, 60, 88, 117, 147, 178, 230	
	9	12, 31, 54, 79, 106, 130, 159, 187, 233	
	10	11, 28, 48, 70, 95, 118, 143, 169, 195, 234	
	11	11, 26, 44, 65, 87, 110, 130, 154, 177, 201, 236	
	12	10, 24, 41, 60, 80, 101, 120, 141, 162, 183, 205, 237	
	42049	3	38, 90, 189
		4	34, 66, 124, 192
5		30, 54, 97, 151, 195	
6		27, 47, 80, 121, 168, 196	
7		26, 43, 70, 103, 138, 174, 196	
8		24, 41, 63, 90, 120, 154, 177, 196	
9		23, 38, 57, 82, 109, 135, 165, 187, 198	
10		22, 37, 53, 74, 97, 121, 147, 171, 198, 188	
11		22, 35, 49, 68, 89, 112, 132, 156, 174, 199, 190	
12		21, 33, 46, 64, 83, 103, 121, 142, 163, 179, 200, 191	
253027		3	68, 103, 150
		4	61, 93, 122, 186
	5	57, 83, 112, 137, 209	
	6	54, 75, 105, 127, 156, 228	
	7	52, 69, 96, 120, 144, 173, 234	
	8	50, 65, 87, 110, 130, 155, 184, 238	
	9	49, 62, 81, 104, 123, 144, 166, 194, 241	
	10	48, 60, 76, 98, 116, 133, 153, 176, 200, 243	
	11	47, 58, 73, 92, 110, 126, 144, 162, 184, 206, 244	
	12	46, 55, 69, 86, 104, 120, 135, 153, 171, 191, 212, 246	

TABLE 2: Continued.

Image	Cluster	Final updated cluster centroids	
169012	3	48, 92, 183	
	4	44, 73, 125, 201	
	5	41, 64, 104, 148, 211	
	6	39, 58, 90, 127, 166, 218	
	7	37, 54, 79, 112, 145, 178, 222	
	8	35, 51, 72, 100, 129, 159, 188, 227	
	9	34, 49, 67, 91, 117, 142, 169, 195, 230	
	10	33, 46, 62, 84, 107, 131, 154, 178, 202, 233	
	11	32, 44, 59, 77, 99, 120, 141, 163, 185, 206, 235	
	12	31, 43, 56, 73, 92, 112, 132, 151, 171, 191, 210, 237	
	210088	3	68, 99, 175
		4	62, 89, 125, 186
5		56, 80, 105, 149, 196	
6		53, 74, 97, 130, 168, 207	
7		50, 70, 92, 115, 149, 178, 213	
8		48, 66, 85, 104, 133, 162, 187, 220	
9		47, 63, 81, 98, 120, 147, 173, 195, 224	
10		46, 60, 77, 94, 112, 135, 159, 180, 200, 227	
11		45, 58, 73, 89, 104, 123, 146, 167, 186, 205, 230	
12		45, 55, 70, 85, 100, 117, 136, 156, 174, 191, 208, 232	
208001		3	40, 81, 157
		4	35, 69, 109, 181
	5	32, 59, 91, 130, 195	
	6	30, 51, 80, 113, 152, 211	
	7	28, 45, 72, 99, 130, 164, 218	
	8	26, 39, 64, 88, 116, 147, 176, 224	
	9	24, 35, 58, 80, 104, 130, 158, 185, 229	
	10	21, 33, 52, 74, 95, 119, 143, 167, 191, 231	
	11	20, 31, 48, 68, 88, 109, 130, 154, 176, 197, 233	
	12	19, 31, 46, 64, 81, 100, 120, 141, 162, 182, 203, 235	
	10081	3	48, 104, 164
		4	38, 74, 122, 166
5		32, 60, 107, 152, 181	
6		27, 54, 89, 127, 177, 153	
7		25, 48, 75, 110, 148, 185, 163	
8		23, 43, 66, 95, 127, 153, 187, 167	
9		21, 40, 61, 87, 115, 146, 171, 193, 159	
10		20, 36, 55, 78, 100, 125, 150, 177, 205, 164	
11		19, 34, 50, 69, 93, 117, 142, 164, 178, 208, 154	
12		18, 31, 48, 65, 86, 105, 126, 148, 169, 181, 211, 159	
155060		3	43, 83, 187
		4	35, 68, 111, 212
	5	29, 56, 91, 131, 220	
	6	23, 49, 80, 113, 150, 223	
	7	19, 44, 70, 99, 129, 168, 226	
	8	17, 39, 62, 89, 117, 145, 185, 228	
	9	15, 36, 56, 80, 105, 129, 156, 194, 229	
	10	14, 33, 51, 72, 95, 119, 142, 169, 201, 231	
	11	13, 31, 48, 67, 88, 109, 129, 151, 179, 208, 232	
	12	12, 29, 44, 61, 80, 100, 119, 139, 161, 186, 211, 233	

TABLE 2: Continued.

Image	Cluster	Final updated cluster centroids	
35070	3	31, 90, 124	
	4	29, 77, 125, 103	
	5	27, 61, 91, 132, 112	
	6	26, 50, 78, 117, 134, 101	
	7	26, 45, 77, 108, 135, 120, 95	
	8	26, 43, 68, 100, 121, 138, 112, 82	
	9	25, 40, 65, 85, 108, 128, 144, 118, 98	
	10	25, 39, 58, 78, 96, 117, 135, 151, 125, 108	
	11	25, 37, 52, 72, 89, 109, 127, 149, 136, 117, 101	
	12	25, 37, 49, 68, 84, 103, 119, 135, 150, 127, 111, 94	
	25098	3	28, 85, 167
		4	21, 68, 119, 182
5		17, 53, 93, 141, 196	
6		15, 47, 82, 122, 160, 209	
7		14, 42, 73, 105, 138, 169, 212	
8		13, 37, 64, 90, 122, 153, 178, 215	
9		12, 34, 57, 81, 109, 136, 163, 189, 221	
10		12, 31, 51, 75, 98, 124, 148, 170, 195, 225	
11		12, 29, 47, 68, 88, 112, 134, 157, 177, 201, 229	
12		11, 27, 44, 64, 82, 102, 124, 145, 165, 185, 209, 234	

the updated cluster centroids are ultimately used to compute the output images in the final step of PICA.

Table 3 shows the weights of clusters from 3 to 12 for all the test images in this study. It can be noted in Table 3 for all the images that cluster weights for a particular image add up to unity. This is in perfect agreement with the probability theory in (10). In codicil, it can be observed in Table 3 that no cluster weight for all the test images is equal to zero. This implies that there is no possibility for the algorithm to break down at any number of clusters and there is no incidence of empty clusters, which can result in the dead centers syndrome using the proposed algorithm.

4.3. Comparative Results. In this section, we adopted both qualitative (subjective) and quantitative (objective) evaluations to compare the segmentation results of the proposed algorithm with KM, PSO, DPSO, and FODPSO segmentation algorithms. These existing algorithms were selected because KM clustering is reported to be one of the most prevalent clustering algorithms due to its implementation simplicity and low computational costs. The PSO-based segmentation methods (PSO, DPSO, and FODPSO) were also shown in the literature to act better than other metaheuristic methods in terms of precision, robustness of results, and runtime [28, 37].

4.3.1. Qualitative. Qualitative evaluation on the basis of human visual perception is a widely used strategy in the literature to carry out performance assessment of image segmentation algorithms [29]. The original grayscale images selected from the Berkeley Segmentation Dataset and Benchmark for evaluations are labelled as (a) in Figures 1–12 while the segmentation outputs by the conventional KM, PSO,

TABLE 3: Cluster weights.

Image	Cluster	Cluster weights	
45077	3	0.24, 0.53, 0.22	
	4	0.16, 0.42, 0.30, 0.12	
	5	0.11, 0.32, 0.37, 0.11, 0.09	
	6	0.08, 0.20, 0.29, 0.18, 0.12, 0.14	
	7	0.05, 0.16, 0.27, 0.18, 0.10, 0.07, 0.17	
	8	0.04, 0.14, 0.22, 0.22, 0.12, 0.07, 0.05, 0.14	
	9	0.03, 0.11, 0.21, 0.21, 0.13, 0.09, 0.05, 0.04, 0.15	
	10	0.02, 0.10, 0.19, 0.22, 0.16, 0.09, 0.06, 0.03, 0.03, 0.11	
	11	0.01, 0.09, 0.13, 0.19, 0.17, 0.12, 0.08, 0.05, 0.03, 0.02, 0.12	
	12	0.01, 0.07, 0.11, 0.14, 0.17, 0.16, 0.09, 0.05, 0.02, 0.03, 0.02, 0.12	
	157055	3	0.17, 0.22, 0.61
		4	0.14, 0.11, 0.23, 0.52
5		0.11, 0.10, 0.16, 0.27, 0.36	
6		0.09, 0.10, 0.10, 0.14, 0.27, 0.30	
7		0.08, 0.09, 0.08, 0.13, 0.19, 0.19, 0.24	
8		0.07, 0.09, 0.06, 0.10, 0.10, 0.21, 0.17, 0.21	
9		0.06, 0.08, 0.05, 0.07, 0.10, 0.13, 0.17, 0.15, 0.17	
10		0.05, 0.08, 0.05, 0.06, 0.09, 0.08, 0.17, 0.14, 0.14, 0.15	
11		0.05, 0.08, 0.05, 0.05, 0.07, 0.08, 0.09, 0.15, 0.13, 0.13, 0.12	
12		0.04, 0.07, 0.05, 0.04, 0.06, 0.08, 0.06, 0.13, 0.13, 0.12, 0.12, 0.10	
78098		3	0.25, 0.34, 0.41
		4	0.18, 0.30, 0.25, 0.28
	5	0.13, 0.25, 0.23, 0.17, 0.23	
	6	0.10, 0.20, 0.22, 0.19, 0.10, 0.19	
	7	0.09, 0.16, 0.20, 0.18, 0.13, 0.09, 0.16	
	8	0.07, 0.14, 0.18, 0.16, 0.15, 0.08, 0.07, 0.15	
	9	0.07, 0.12, 0.16, 0.16, 0.14, 0.10, 0.07, 0.06, 0.14	
	10	0.06, 0.10, 0.13, 0.15, 0.13, 0.12, 0.08, 0.06, 0.05, 0.13	
	11	0.06, 0.08, 0.12, 0.14, 0.13, 0.11, 0.09, 0.06, 0.05, 0.04, 0.12	
	12	0.05, 0.07, 0.11, 0.13, 0.11, 0.11, 0.10, 0.06, 0.05, 0.04, 0.04, 0.12	
	42049	3	0.10, 0.09, 0.81
		4	0.07, 0.07, 0.09, 0.77
5		0.05, 0.07, 0.06, 0.11, 0.71	
6		0.04, 0.07, 0.05, 0.06, 0.14, 0.65	
7		0.03, 0.06, 0.04, 0.04, 0.06, 0.13, 0.63	
8		0.02, 0.06, 0.04, 0.04, 0.04, 0.07, 0.08, 0.64	
9		0.02, 0.05, 0.04, 0.03, 0.03, 0.04, 0.09, 0.16, 0.52	
10		0.02, 0.05, 0.04, 0.03, 0.03, 0.04, 0.04, 0.09, 0.52, 0.15	
11		0.02, 0.04, 0.04, 0.03, 0.03, 0.03, 0.03, 0.05, 0.07, 0.41, 0.26	
12		0.01, 0.04, 0.04, 0.03, 0.03, 0.02, 0.03, 0.03, 0.06, 0.07, 0.37, 0.270	
253027		3	0.26, 0.37, 0.38
		4	0.16, 0.35, 0.35, 0.15
	5	0.10, 0.27, 0.35, 0.18, 0.09	
	6	0.07, 0.22, 0.33, 0.24, 0.08, 0.06	
	7	0.05, 0.17, 0.29, 0.30, 0.11, 0.03, 0.05	
	8	0.03, 0.14, 0.21, 0.30, 0.18, 0.07, 0.02, 0.05	
	9	0.02, 0.12, 0.17, 0.27, 0.24, 0.09, 0.04, 0.02, 0.04	
	10	0.02, 0.10, 0.15, 0.21, 0.25, 0.13, 0.06, 0.02, 0.01, 0.04	
	11	0.01, 0.08, 0.13, 0.17, 0.24, 0.19, 0.07, 0.03, 0.02, 0.01, 0.04	
	12	0.01, 0.07, 0.12, 0.14, 0.21, 0.21, 0.10, 0.05, 0.02, 0.01, 0.01, 0.04	

TABLE 3: Continued.

Image	Cluster	Cluster weights	
169012	3	0.39, 0.27, 0.34	
	4	0.29, 0.27, 0.20, 0.24	
	5	0.23, 0.27, 0.17, 0.15, 0.19	
	6	0.18, 0.26, 0.16, 0.14, 0.11, 0.15	
	7	0.14, 0.25, 0.16, 0.13, 0.11, 0.09, 0.13	
	8	0.10, 0.24, 0.16, 0.12, 0.11, 0.09, 0.08, 0.11	
	9	0.09, 0.21, 0.17, 0.11, 0.09, 0.08, 0.07, 0.07, 0.10	
	10	0.07, 0.20, 0.17, 0.11, 0.09, 0.09, 0.07, 0.06, 0.06, 0.08	
	11	0.06, 0.17, 0.18, 0.11, 0.09, 0.08, 0.07, 0.06, 0.06, 0.05, 0.08	
	12	0.05, 0.15, 0.17, 0.12, 0.08, 0.08, 0.07, 0.06, 0.05, 0.05, 0.05, 0.07	
	210088	3	0.33, 0.46, 0.20
		4	0.21, 0.48, 0.16, 0.15
5		0.12, 0.38, 0.29, 0.11, 0.11	
6		0.07, 0.32, 0.33, 0.12, 0.09, 0.07	
7		0.05, 0.27, 0.33, 0.15, 0.08, 0.07, 0.05	
8		0.03, 0.20, 0.31, 0.21, 0.09, 0.07, 0.06, 0.04	
9		0.03, 0.15, 0.28, 0.24, 0.10, 0.07, 0.06, 0.04, 0.03	
10		0.02, 0.12, 0.26, 0.26, 0.12, 0.07, 0.06, 0.05, 0.03, 0.02	
11		0.02, 0.09, 0.21, 0.26, 0.15, 0.08, 0.06, 0.05, 0.04, 0.03, 0.02	
12		0.01, 0.07, 0.18, 0.25, 0.19, 0.08, 0.05, 0.05, 0.05, 0.03, 0.02, 0.02	
208001		3	0.33, 0.43, 0.24
		4	0.23, 0.40, 0.22, 0.14
	5	0.18, 0.32, 0.28, 0.12, 0.10	
	6	0.13, 0.25, 0.30, 0.17, 0.08, 0.07	
	7	0.10, 0.22, 0.28, 0.19, 0.09, 0.06, 0.06	
	8	0.05, 0.20, 0.25, 0.22, 0.13, 0.06, 0.04, 0.05	
	9	0.03, 0.18, 0.22, 0.23, 0.14, 0.08, 0.05, 0.03, 0.04	
	10	0.01, 0.16, 0.19, 0.23, 0.16, 0.09, 0.05, 0.04, 0.02, 0.04	
	11	0.01, 0.14, 0.17, 0.20, 0.18, 0.11, 0.07, 0.05, 0.03, 0.02, 0.03	
	12	0.01, 0.14, 0.14, 0.19, 0.17, 0.12, 0.08, 0.05, 0.04, 0.02, 0.02, 0.03	
	10081	3	0.08, 0.22, 0.70
		4	0.04, 0.12, 0.17, 0.66
5		0.02, 0.09, 0.17, 0.43, 0.29	
6		0.01, 0.08, 0.10, 0.16, 0.37, 0.28	
7		0.01, 0.05, 0.08, 0.14, 0.30, 0.21, 0.22	
8		0.01, 0.04, 0.07, 0.09, 0.14, 0.31, 0.19, 0.16	
9		0.01, 0.03, 0.06, 0.07, 0.11, 0.24, 0.18, 0.12, 0.18	
10		0.005, 0.02, 0.06, 0.06, 0.07, 0.11, 0.28, 0.16, 0.06, 0.18	
11		0.004, 0.02, 0.04, 0.05, 0.07, 0.09, 0.17, 0.21, 0.15, 0.05, 0.15	
12		0.003, 0.01, 0.04, 0.05, 0.05, 0.06, 0.09, 0.22, 0.14, 0.12, 0.04, 0.16	
155060		3	0.23, 0.32, 0.45
		4	0.13, 0.32, 0.23, 0.33
	5	0.07, 0.27, 0.23, 0.15, 0.29	
	6	0.04, 0.22, 0.24, 0.16, 0.08, 0.27	
	7	0.02, 0.18, 0.21, 0.17, 0.11, 0.05, 0.26	
	8	0.02, 0.13, 0.20, 0.19, 0.12, 0.06, 0.05, 0.24	
	9	0.01, 0.10, 0.18, 0.17, 0.13, 0.08, 0.04, 0.05, 0.23	
	10	0.01, 0.07, 0.15, 0.17, 0.15, 0.10, 0.05, 0.03, 0.06, 0.21	
	11	0.01, 0.06, 0.14, 0.15, 0.14, 0.11, 0.07, 0.04, 0.03, 0.07, 0.19	
	12	0.01, 0.04, 0.12, 0.15, 0.13, 0.12, 0.09, 0.05, 0.03, 0.03, 0.07, 0.18	

TABLE 3: Continued.

Image	Cluster	Cluster weights	
35070	3	0.10, 0.20, 0.70	
	4	0.09, 0.11, 0.62, 0.18	
	5	0.08, 0.06, 0.11, 0.37, 0.38	
	6	0.08, 0.04, 0.06, 0.34, 0.30, 0.18	
	7	0.07, 0.03, 0.08, 0.24, 0.28, 0.24, 0.06	
	8	0.07, 0.03, 0.04, 0.17, 0.31, 0.21, 0.13, 0.04	
	9	0.07, 0.03, 0.04, 0.07, 0.17, 0.21, 0.11, 0.24, 0.07	
	10	0.07, 0.02, 0.02, 0.06, 0.09, 0.19, 0.11, 0.06, 0.20, 0.17	
	11	0.07, 0.02, 0.02, 0.05, 0.07, 0.11, 0.22, 0.06, 0.06, 0.24, 0.09	
	12	0.07, 0.02, 0.02, 0.03, 0.05, 0.10, 0.22, 0.10, 0.06, 0.15, 0.15, 0.05	
	25098	3	0.23, 0.36, 0.41
		4	0.16, 0.30, 0.25, 0.29
5		0.13, 0.20, 0.25, 0.23, 0.19	
6		0.12, 0.16, 0.23, 0.19, 0.18, 0.12	
7		0.11, 0.13, 0.20, 0.16, 0.16, 0.13, 0.11	
8		0.10, 0.11, 0.16, 0.16, 0.16, 0.14, 0.08, 0.09	
9		0.09, 0.09, 0.12, 0.17, 0.13, 0.13, 0.13, 0.06, 0.07	
10		0.09, 0.08, 0.11, 0.15, 0.12, 0.13, 0.12, 0.10, 0.05, 0.06	
11		0.08, 0.07, 0.09, 0.12, 0.13, 0.11, 0.11, 0.11, 0.08, 0.05, 0.05	
12		0.08, 0.06, 0.09, 0.11, 0.12, 0.10, 0.11, 0.10, 0.10, 0.06, 0.05, 0.04	

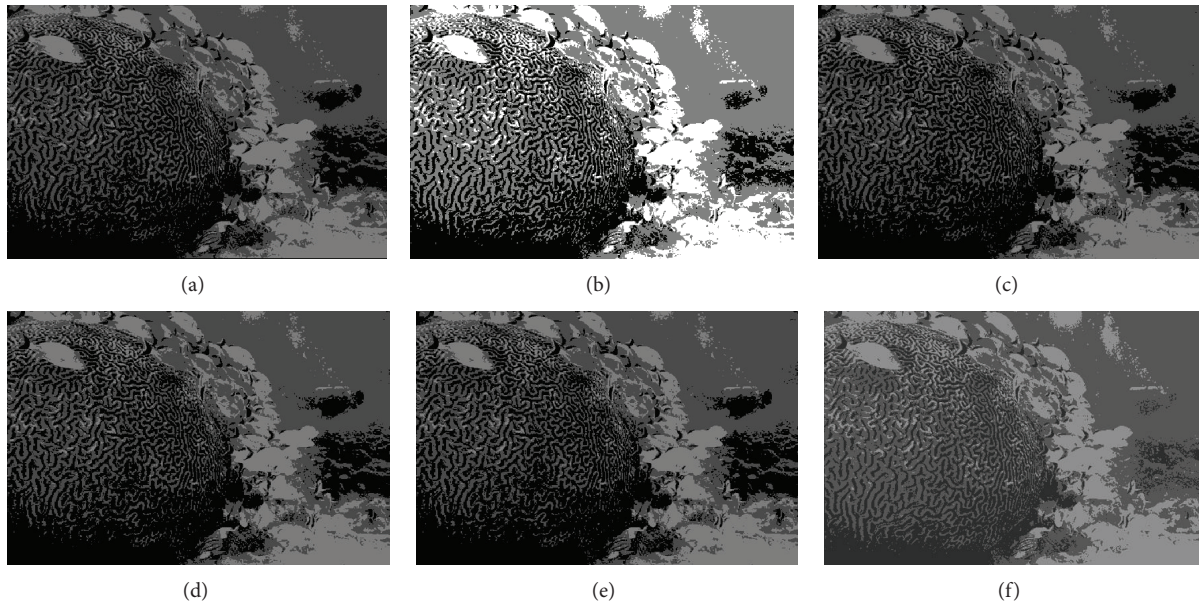


FIGURE 1: Segmentation results in 3 clusters/levels of image “45077” after applying different algorithms: (a) original image, (b) KM, (c) PSO, (d) DPSO, (e) FODPSO, and (f) proposed.

DPSO, FODPSO, and the proposed algorithm are labelled as (b) to (f), respectively. The number of clusters for segmenting each of the test images varied from 3 to 14. Worthy of note is the fact that, based on visual appeal, the segmentation outputs of all the conventional algorithms and our proposed algorithm are only fairly acceptable at cluster/level 3. In

general, there were improvements in the visual appeal of the outputs of the conventional algorithms and the proposed algorithm as we increased the number of clusters/levels from 4 up to 14. However, it can be observed that there are several white patches in the outputs of the KM algorithm as conspicuously illustrated in Figures 2, 3, 4, 5, 7, 8, and

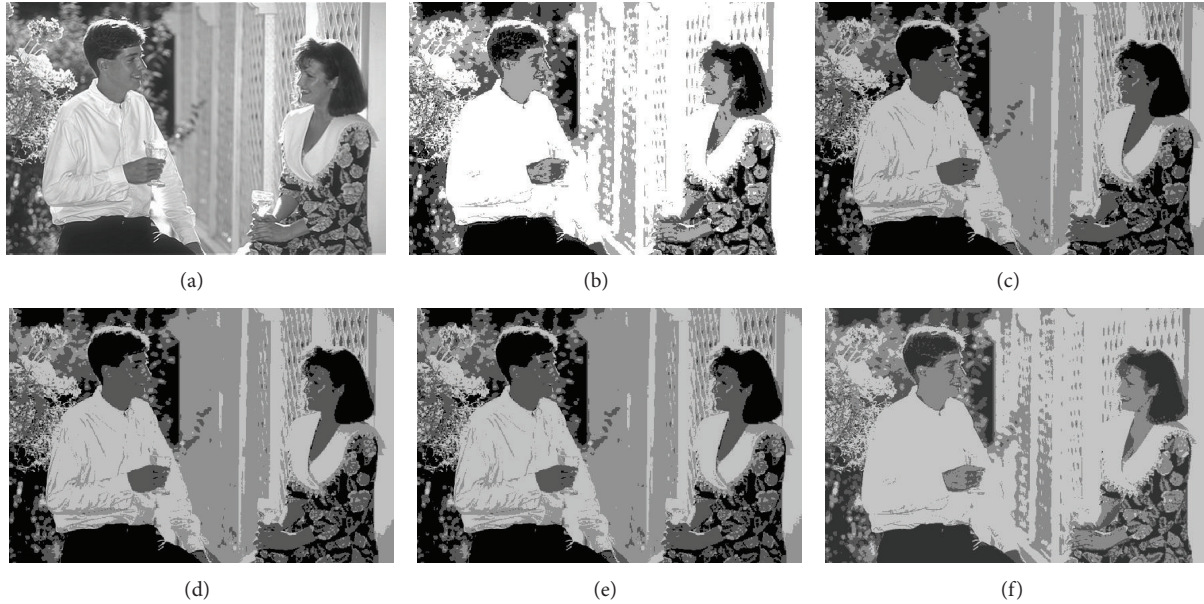


FIGURE 2: Segmentation results in 4 clusters/levels of image “157055” after applying different algorithms: (a) original image, (b) KM, (c) PSO, (d) DPSO, (e) FODPSO, and (f) proposed.

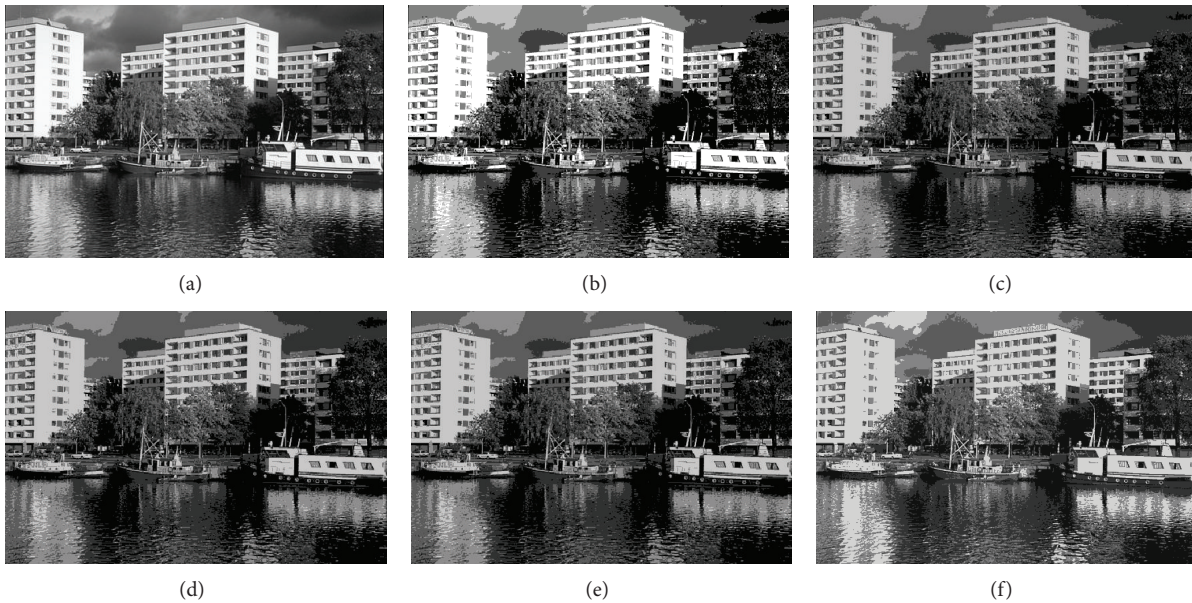


FIGURE 3: Segmentation results in 5 clusters/levels of image “78098” after applying different algorithms: (a) original image, (b) KM, (c) PSO, (d) DPSO, (e) FODPSO, and (f) proposed.

11. The segmentation outputs of PSO, DPSO, and FODPSO algorithms also have a lot of black patches as noticeably shown in Figures 2, 3, 4, 5, 6, 7, 8, 11, and 12. Conversely, the output of the proposed algorithm is shown across the entire test images and from clusters 4 to 14 to be more visually appealing because no white or black patches are found in any of the results. This qualitative evaluation clearly shows that our algorithm achieved more homogeneous segmentation outputs than the other comparative algorithms in this study. Quantitative evaluation is further carried out for the

selected test images using the conventional algorithms and the proposed algorithm.

4.3.2. *Quantitative.* Quantitative evaluation objectively computes the performance of segmentation algorithms with appropriate similarity metrics and it is not subject to human errors like in the qualitative evaluation method. Consequently, for the quantitative aspect of this study, we employed some metrics to compare the proposed algorithm with the other algorithms. These metrics are the Jaccard index (J)

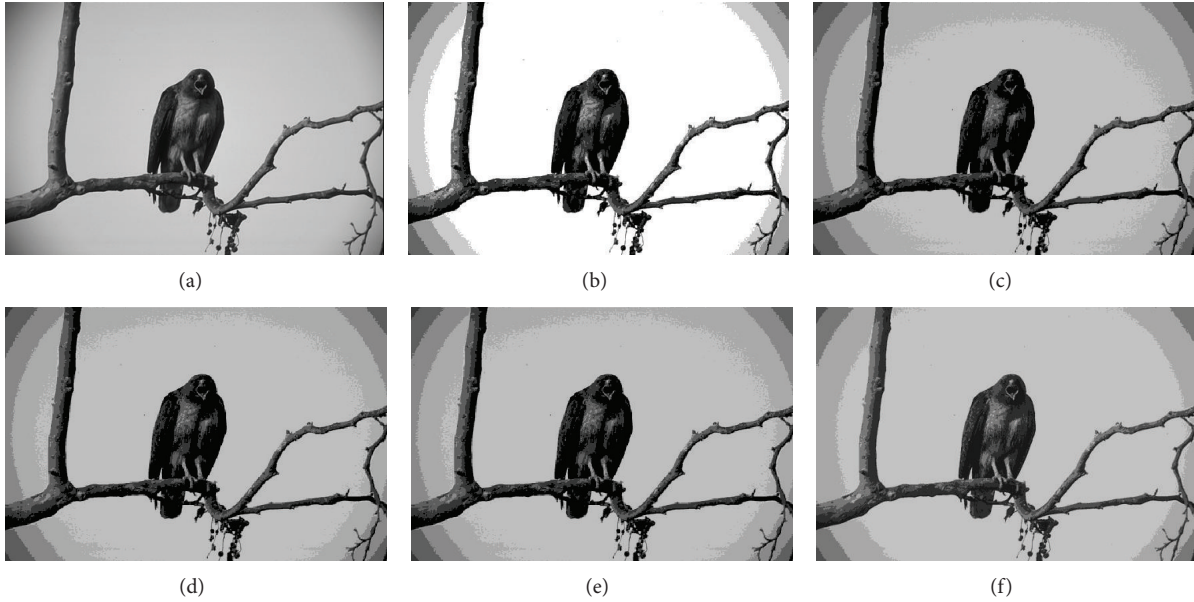


FIGURE 4: Segmentation results in 6 clusters/levels of image “42049” after applying different algorithms: (a) original image, (b) KM, (c) PSO, (d) DPSO, (e) FODPSO, and (f) proposed.

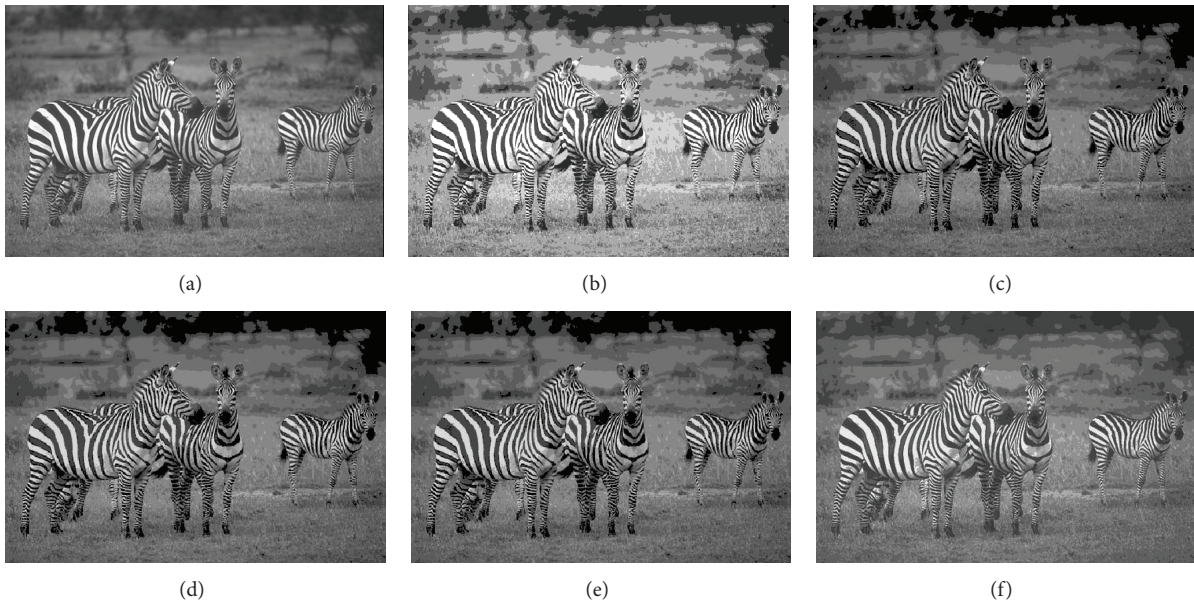


FIGURE 5: Segmentation results in 7 clusters/levels of image “253027” after applying different algorithms: (a) original image, (b) KM, (c) PSO, (d) DPSO, (e) FODPSO, and (f) proposed.

and the Structural Similarity Measure (SSIM). The maximum Jaccard index and SSIM of 1 are only achieved if the two images are identical. These similarity metrics (Jaccard and SSIM) can be mathematically defined in terms of two images $x = \{x_i \mid i = 1, \dots, M\}$ and $y = \{y_i \mid i = 1, \dots, N\}$.

Given that $|x|$ denotes the cardinality of image x , which is a count of the number of elements that are present in x , the

Jaccard similarity index between the two images x and y is given as [49]

$$J(x, y) = \frac{|x \cap y|}{|x \cup y|}, \quad (11)$$

where $x \cap y$ denotes the intersection between the two images and represents all elements that are in both images, while $x \cup y$

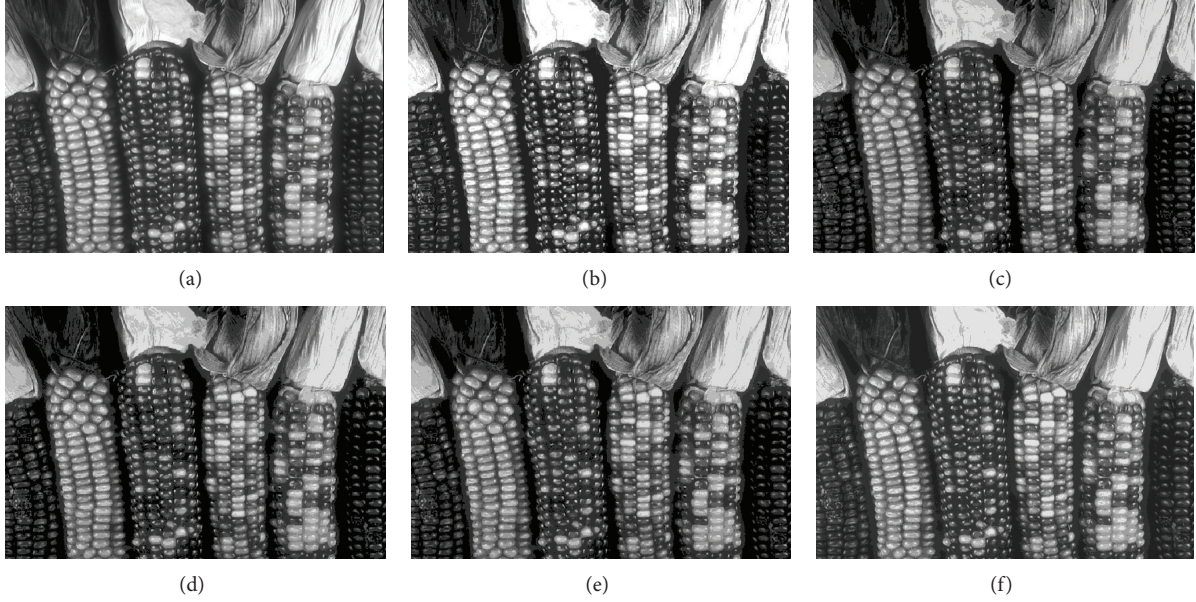


FIGURE 6: Segmentation results in 8 clusters/levels of image “169012” after applying different algorithms: (a) original image, (b) KM, (c) PSO, (d) DPSO, (e) FODPSO, and (f) proposed.

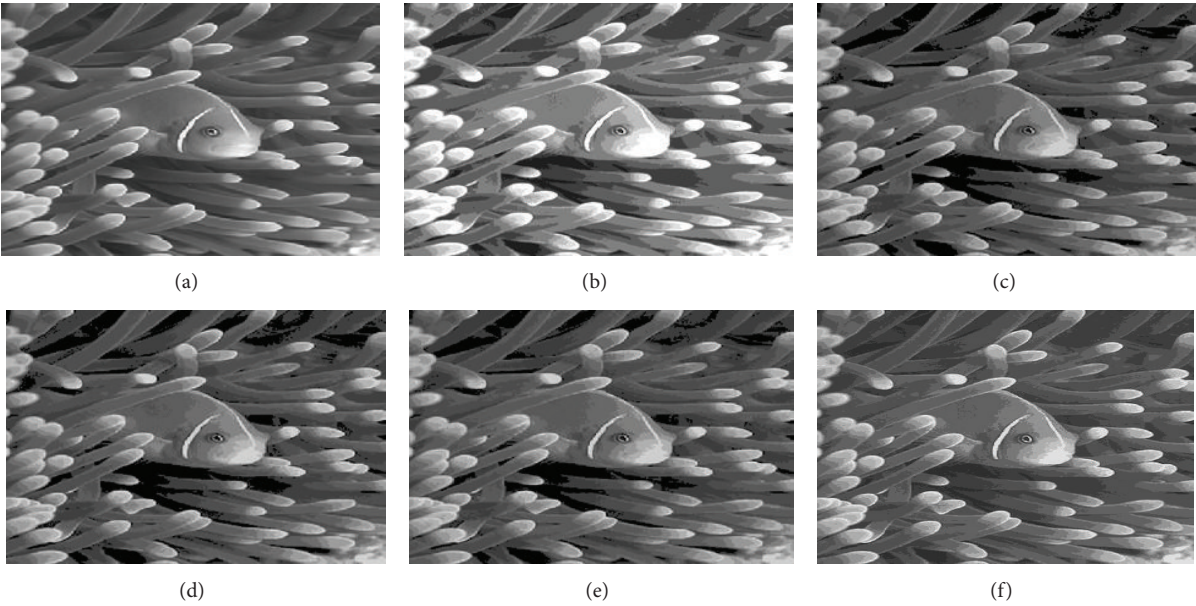


FIGURE 7: Segmentation results in 9 clusters/levels of image “210088” after applying different algorithms: (a) original image, (b) KM, (c) PSO, (d) DPSO, (e) FODPSO, and (f) proposed.

denotes the union between the two images and represents all elements that are in either of them.

The SSIM index was proposed to predict human preferences in image quality assessment. To compute SSIM, the means (μ_x, μ_y) , the variances (σ_x^2, σ_y^2) , and the cross-covariance (σ_{xy}) of images x and y are first computed and are

based on these values, and the SSIM between images x and y is given as [50]

$$S(x, y) = \frac{(2\mu_x\mu_y + C_1)(2\sigma_{xy} + C_2)}{(\mu_x^2 + \mu_y^2 + C_1)(\sigma_x^2 + \sigma_y^2 + C_2)}, \quad (12)$$

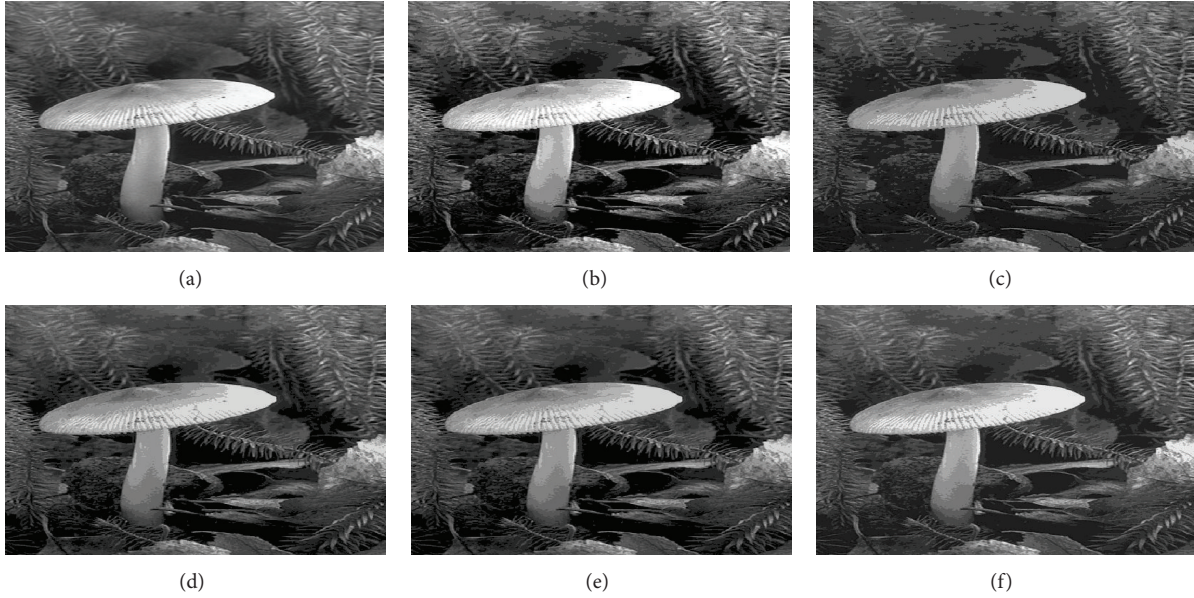


FIGURE 8: Segmentation results in 10 clusters/levels of image “208001” after applying different algorithms: (a) original image, (b) KM, (c) PSO, (d) DPSO, (e) FODPSO, and (f) proposed.

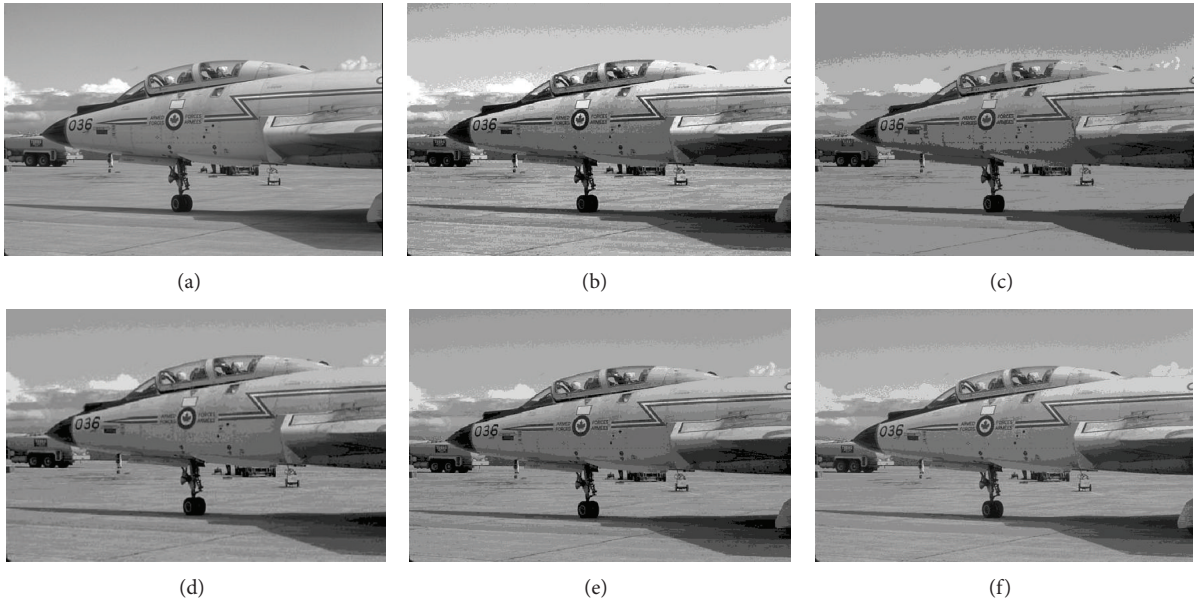


FIGURE 9: Segmentation results in 11 clusters/levels of image “10081” after applying different algorithms: (a) original image, (b) KM, (c) PSO, (d) DPSO, (e) FODPSO, and (f) proposed.

where C_1 and C_2 are small positive constants, μ_x is the mean of x , and σ_x^2 is the variance.

The values obtained for these metrics in (11) and (12) when applied to the test images for clusters 3 to 14 are shown in Table 4. As shown in the table, both the Jaccard index and the SSIM index for the proposed algorithm improved progressively from cluster 3 up to cluster 14 for the different test images. In addition, the results of the two metrics for the proposed algorithm are better than the values obtained for the other algorithms compared from clusters/levels 3 up to

14 across all the test images (Table 4). These results further consolidate the qualitative comparison result, which earlier established that our proposed algorithm performs better than KM, PSO, DPSO, and FODPSO. The computed evaluation metrics also indicate that the values of the SSIM indices are consistently higher than the values of Jaccard indices for all the test images from clusters/levels 3 up to 14. For instance, at cluster 3 in Table 4, the Jaccard index for the proposed algorithm is 0.8639 while that of the SSIM index is 0.8979 and at cluster 14, the value of the Jaccard index is 0.9603

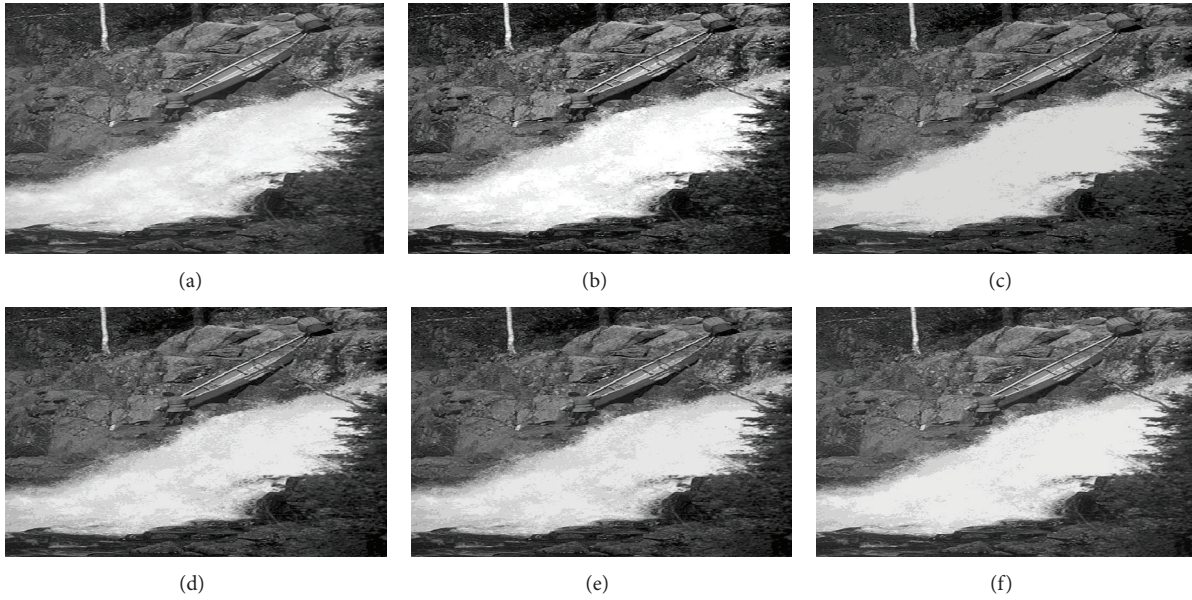


FIGURE 10: Segmentation results in 12 clusters/levels of image “155060” after applying different algorithms: (a) original image, (b) KM, (c) PSO, (d) DPSO, (e) FODPSO, and (f) proposed.

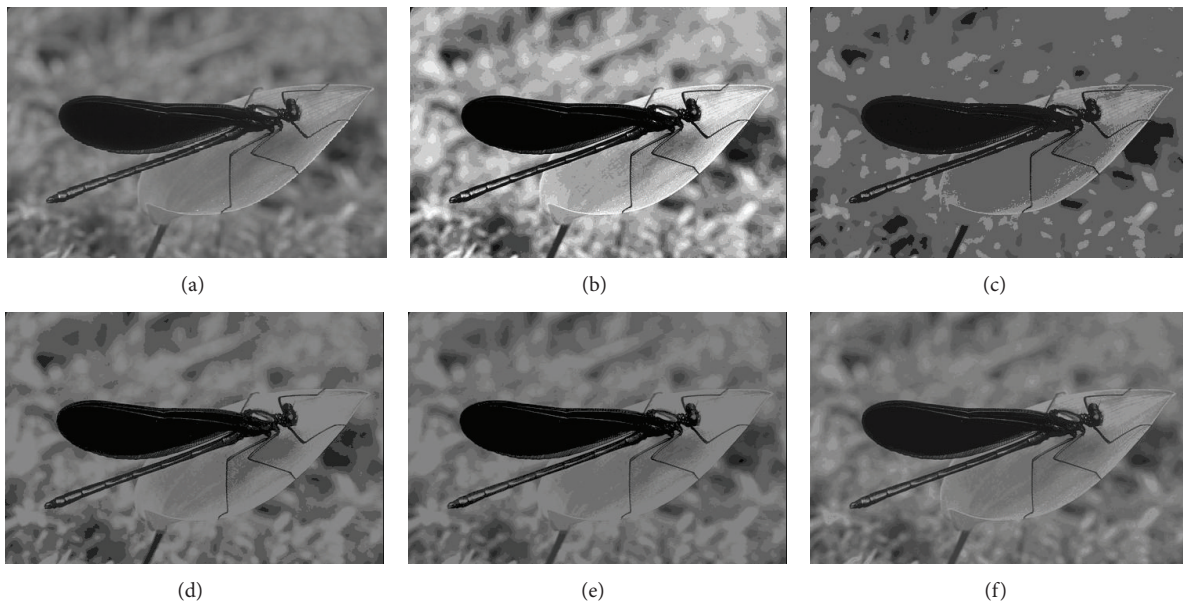


FIGURE 11: Segmentation results in 13 clusters/levels of image “35070” after applying different algorithms: (a) original image, (b) KM, (c) PSO, (d) DPSO, (e) FODPSO, and (f) proposed.

while that of the SSIM index is 0.9965. A similar trend was observed for all the conventional algorithms, even though the values obtained from the two metrics were lower for the conventional algorithms than the proposed algorithm. Apparently, the SSIM index value of 0.9965 obtained for the proposed algorithm at cluster 14 is a better quantitative representation of the visual appeal of the segmented image than the Jaccard index value of 0.9603. We can therefore safely infer that, based on the evaluations carried out in this study, the SSIM index is a better measure of similarity between an

input image and a segmented image than the Jaccard index. Hence, the SSIM evaluation metric is highly promising for many other post-image segmentation processing tasks such as object features extraction and content retrieval.

5. Conclusion

In this study, a new clustering algorithm was proposed and applied to multilevel image segmentation problem. The objectives of the proposed algorithm were to improve the

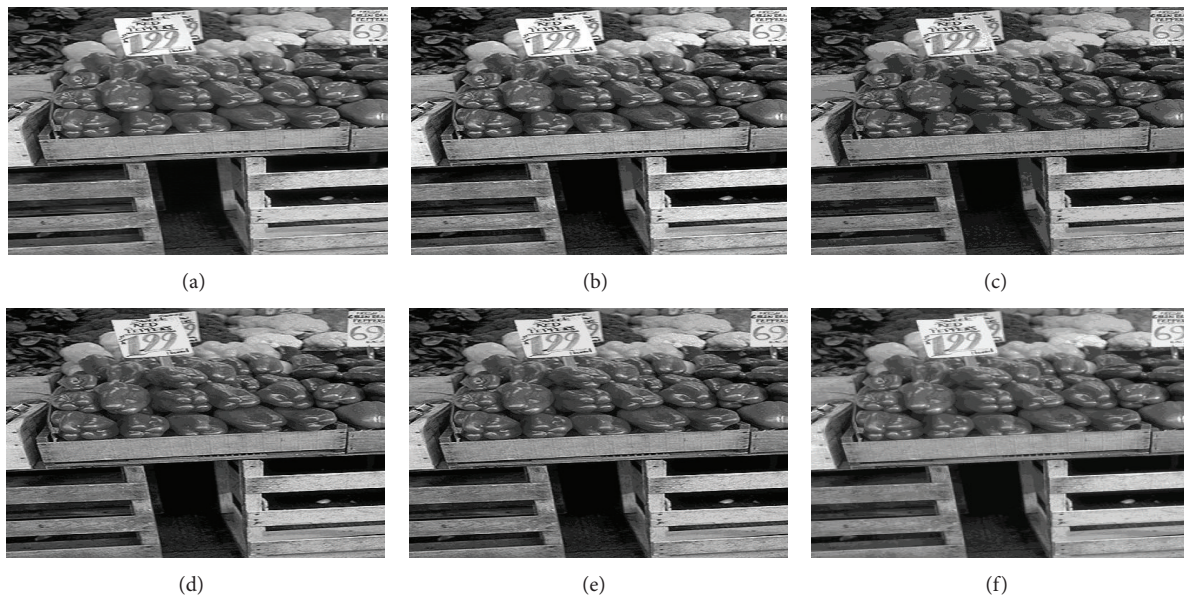


FIGURE 12: Segmentation results in 14 clusters/levels of image “25098” after applying different algorithms: (a) original image, (b) KM, (c) PSO, (d) DPSO, (e) FODPSO, and (f) proposed.

TABLE 4: Comparative results.

Image	Q	Clusters	Metrics	KM	PSO	DPSO	FODPSO	Proposed
45077	240	3	Jaccard	0.5560	0.6257	0.5963	0.6251	0.8639
			SSIM	0.7682	0.6917	0.6756	0.7220	0.8979
157055	223	4	Jaccard	0.8081	0.7881	0.7889	0.7889	0.9004
			SSIM	0.8204	0.8091	0.8082	0.8082	0.9418
78098	253	5	Jaccard	0.8303	0.7682	0.7682	0.7685	0.8802
			SSIM	0.8569	0.7324	0.7324	0.8229	0.9669
42049	233	6	Jaccard	0.8465	0.9212	0.9213	0.9213	0.9646
			SSIM	0.9082	0.9238	0.9237	0.9237	0.9894
253027	222	7	Jaccard	0.7956	0.8427	0.8347	0.8573	0.9410
			SSIM	0.8791	0.9113	0.8997	0.9356	0.9787
169012	235	8	Jaccard	0.8272	0.8391	0.8307	0.8306	0.9377
			SSIM	0.7983	0.8530	0.8312	0.8311	0.9910
210088	221	9	Jaccard	0.8214	0.8876	0.8778	0.8960	0.9521
			SSIM	0.9655	0.9329	0.9183	0.9643	0.9894
208001	247	10	Jaccard	0.8210	0.8581	0.8624	0.8581	0.9383
			SSIM	0.8272	0.8814	0.8940	0.8806	0.9911
10081	249	11	Jaccard	0.9157	0.9350	0.9395	0.9401	0.9681
			SSIM	0.9765	0.9872	0.9761	0.9766	0.9881
155060	253	12	Jaccard	0.9080	0.9257	0.9246	0.9229	0.9592
			SSIM	0.9465	0.9797	0.9751	0.9760	0.9965
35070	204	13	Jaccard	0.7240	0.8411	0.9133	0.9093	0.9770
			SSIM	0.8501	0.9606	0.9176	0.9167	0.9937
25098	252	14	Jaccard	0.8218	0.8071	0.8320	0.8324	0.9603
			SSIM	0.8845	0.9335	0.9188	0.9523	0.9965

initialization of cluster centroids and the allocation of pixel intensities into clusters. This is to eliminate the dead center problem and inappropriate pixel allocation to clusters as commonly encountered in many of the existing clustering based multilevel segmentation methods. The simple mathematical concepts utilized in achieving the objectives are linear partitioning of the pixel intensity set and between-cluster variance criterion function. The new multilevel segmentation algorithm is conceptually simple, robust, and computationally cost effective. The algorithm was compared with KM, PSO, DPSO, and FODPSO on 12 real images from the Berkeley Segmentation Dataset and Benchmark. The qualitative results show that the proposed algorithm consistently produced patch-free segmentation, unlike the other existing algorithms. The quantitative results using the Jaccard index and the SSIM show that the segmentation results of our algorithm improve with increasing number of clusters across different images without a corresponding increase in computational cost, unlike the other algorithms. Our experiments further showed that when the number of clusters K is equal to the number of pixel intensities Q , ($K = Q$ and $Q \leq 256$), the value of SSIM becomes 1, which is a confirmation of the survivability and recoverability capabilities of the algorithm. On the contrary, the other comparative algorithms in this study either break down or become unbearably slow for $K > 180$. This study opens new perspective on multilevel image segmentation because multilevel thresholding algorithms were previously considered suitable for solving multilevel image segmentation problem. Future work will involve a search for better initialization schemes and pixel intensities allocation concepts to further enhance the performance of the algorithm.

Conflict of Interests

The authors declare that there is no conflict of interests regarding the publication of this paper.

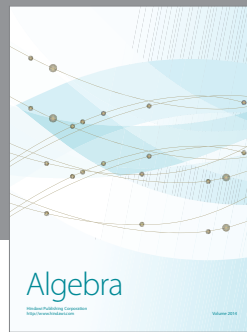
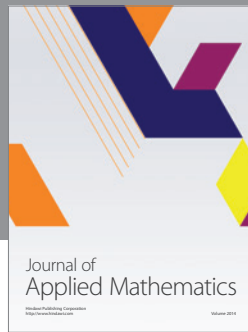
Acknowledgment

E. Adetiba is on postdoctoral fellowship at the ICT and Society (ICTAS) Research Group, Durban University of Technology, South Africa, funded by the Durban University of Technology Research and Development Directorate. He is on postdoctoral research leave from the Department of Electrical & Information Engineering, College of Engineering, Covenant University, Ota, Ogun State, Nigeria.

References

- [1] A. Alihodzic and M. Tuba, "Improved bat algorithm applied to multilevel image thresholding," *The Scientific World Journal*, vol. 2014, Article ID 176718, 16 pages, 2014.
- [2] M. H. J. Vala and A. Baxi, "A review on Otsu image segmentation algorithm," *International Journal of Advanced Research in Computer Engineering & Technology*, vol. 2, no. 2, pp. 387–389, 2013.
- [3] C. A. Glasbey and G. W. Horgan, *Image Analysis for the Biological Sciences*, vol. 1, Wiley, Chichester, UK, 1995.
- [4] D. A. Okuboyejo, O. O. Olugbara, and S. A. Odunaike, "CLAHE inspired segmentation of dermoscopic images using mixture of methods," in *Transactions on Engineering Technologies*, pp. 355–365, Springer, Dordrecht, The Netherlands, 2014.
- [5] S. A. Daramola, E. Adetiba, A. U. Adoghe, J. A. Badejo, I. A. Samuel, and T. Fagorusi, "Automatic vehicle identification system using license plate," *International Journal of Engineering Science and Technology*, vol. 3, no. 2, pp. 1712–1719, 2011.
- [6] Y. Ramadevi, T. Sridevi, B. Poornima, and B. Kalyani, "Segmentation and object recognition using edge detection technique," *International Journal of Computer Science & Information Technology*, vol. 2, no. 6, pp. 153–161, 2010.
- [7] D. Oliva, E. Cuevas, G. Pajares, D. Zaldivar, and V. Osuna, "A multilevel thresholding algorithm using electro-magnetism optimization," *Neurocomputing*, vol. 139, pp. 357–381, 2014.
- [8] B. T. Abe, O. O. Olugbara, and T. Marwala, "Experimental comparison of support vector machines with random forests for hyperspectral image land cover classification," *Journal of Earth System Science*, vol. 123, no. 4, pp. 779–790, 2014.
- [9] H. B. Kekre and S. M. Gharge, "Image segmentation using extended edge operator for mammographic images," *International Journal on Computer Science and Engineering*, vol. 2, no. 4, pp. 1086–1091, 2010.
- [10] G. C. Lekhana and R. Srikantaswamy, "Real time license plate recognition system," *International Journal of Advanced Technology & Engineering Research*, vol. 2, no. 4, pp. 5–9, 2012.
- [11] T. Zuva, O. O. Olugbara, S. O. Ojo, and S. M. Ngwira, "Image segmentation, available techniques, developments and open issues," *Canadian Journal on Image Processing and Computer Vision*, vol. 2, no. 3, pp. 20–29, 2011.
- [12] M. Juneja and P. S. Sandhu, "Performance evaluation of edge detection techniques for images in spatial domain," *International Journal of Computer Theory and Engineering*, vol. 1, no. 5, pp. 614–621, 2009.
- [13] M. A. El-Sayed, "A new algorithm based entropic threshold for edge detection in images," *International Journal of Computer Science Issues*, vol. 8, no. 1, pp. 71–78, 2011.
- [14] H. D. Cheng, X. H. Jiang, Y. Sun, and J. Wang, "Color image segmentation: advances and prospects," *Pattern Recognition*, vol. 34, no. 12, pp. 2259–2281, 2001.
- [15] Y.-H. Kuan, C.-M. Kuo, and N.-C. Yang, "Color-based image salient region segmentation using novel region merging strategy," *IEEE Transactions on Multimedia*, vol. 10, no. 5, pp. 832–845, 2008.
- [16] R. C. Gonzalez and R. E. Woods, *Digital Image Processing*, Publishing House of Electronics Industry, Beijing, China, 2nd edition, 2007.
- [17] V. Osuna-Enciso, E. Cuevas, and H. Sossa, "A comparison of nature inspired algorithms for multi-threshold image segmentation," *Expert Systems with Applications*, vol. 40, no. 4, pp. 1213–1219, 2013.
- [18] L. Dong, G. Yu, P. Ogunbona, and W. Li, "An efficient iterative algorithm for image thresholding," *Pattern Recognition Letters*, vol. 29, no. 9, pp. 1311–1316, 2008.
- [19] P.-S. Liao, T.-S. Chen, and P.-C. Chung, "A fast algorithm for multilevel thresholding," *Journal of Information Science and Engineering*, vol. 17, no. 5, pp. 713–727, 2001.
- [20] X. Yang, X. Shen, J. Long, and H. Chen, "An improved median-based Otsu image thresholding algorithm," *AASRI Procedia*, vol. 3, pp. 468–473, 2012.

- [21] N. Otsu, "A threshold selection method from gray-level histograms," *IEEE Transactions on Systems, Man and Cybernetics*, vol. 9, no. 1, pp. 62–66, 1979.
- [22] M. K. Quweider, J. D. Scargle, and B. Jackson, "Grey level reduction for segmentation, thresholding and binarisation of images based on optimal partitioning on an interval," *IET Image Processing*, vol. 1, no. 2, pp. 103–111, 2007.
- [23] D.-Y. Huang, T.-W. Lin, and W.-C. Hu, "Automatic multilevel thresholding based on two-stage Otsu's method with cluster determination by valley estimation," *International Journal of Innovative Computing, Information and Control*, vol. 7, no. 10, pp. 5631–5644, 2011.
- [24] A. M. Khan and S. Ravi, "Image segmentation methods: a comparative study," *International Journal of Soft Computing and Engineering*, vol. 3, no. 4, pp. 84–92, 2013.
- [25] Y. Zhang, "An overview of image and video segmentation in the last 40 years," in *Advances in Image and Video Segmentation*, pp. 1–15, IRM Press, 2006.
- [26] A. Oliver, X. Munoz, J. Battle, L. Pacheco, and J. Freixenet, "Improving clustering algorithms for image segmentation using contour and region information," in *Proceedings of the IEEE International Conference on Automation, Quality and Testing, Robotics*, vol. 2, pp. 315–320, May 2006.
- [27] H. P. Narkhede, "Review of image segmentation techniques," *International Journal of Science and Modern Engineering*, vol. 1, no. 8, pp. 54–61, 2013.
- [28] S. Nilima, P. Dhanesh, and J. Anjali, "Review on image segmentation, clustering and boundary encoding," *International Journal of Innovative Research in Science, Engineering and Technology*, vol. 2, no. 11, pp. 6309–6314, 2013.
- [29] F. U. Siddiqui and N. A. M. Isa, "Optimized K-means (OKM) clustering algorithm for image segmentation," *Opto-electronics Review*, vol. 20, no. 3, pp. 216–225, 2012.
- [30] H. Shamsi and H. Seyedarabi, "A modified fuzzy C-means clustering with spatial information for image segmentation," *International Journal of Computer Theory and Engineering*, vol. 4, no. 5, pp. 762–766, 2012.
- [31] D.-Y. Huang and C.-H. Wang, "Optimal multi-level thresholding using a two-stage Otsu optimization approach," *Pattern Recognition Letters*, vol. 30, no. 3, pp. 275–284, 2009.
- [32] H. Lei, S. Cheng, M.-S. Ao, and Y.-Q. Wu, "Application of an improved genetic algorithm in image segmentation," in *Proceedings of the International Conference on Computer Science and Software Engineering (CSSE '08)*, pp. 898–901, December 2008.
- [33] X. Zhao, M.-E. Lee, and S.-H. Kim, "Improved image segmentation method based on optimized threshold using genetic algorithm," in *Proceedings of the 6th IEEE/ACS International Conference on Computer Systems and Applications (AICCSA '08)*, pp. 921–922, Doha, Qatar, April 2008.
- [34] Q. B. Truong and B. R. Lee, "Automatic multi-thresholds selection for image segmentation based on evolutionary approach," *International Journal of Control, Automation and Systems*, vol. 11, no. 4, pp. 834–844, 2013.
- [35] E. Cuevas, D. Zaldivar, and M. Pérez-Cisneros, "A novel multi-threshold segmentation approach based on differential evolution optimization," *Expert Systems with Applications*, vol. 37, no. 7, pp. 5265–5271, 2010.
- [36] P. Ghamisi, M. S. Couceiro, F. M. L. Martins, and J. A. Benediktsson, "Multilevel image segmentation based on fractional-order darwinian particle swarm optimization," *IEEE Transactions on Geoscience and Remote Sensing*, vol. 52, no. 5, pp. 2382–2394, 2014.
- [37] K. Harnrnouche, M. Diaf, and P. Siarry, "A comparative study of various meta-heuristic techniques applied to the multilevel thresholding problem," *Engineering Applications of Artificial Intelligence*, vol. 23, no. 5, pp. 676–688, 2010.
- [38] J. Tillett, T. M. Rao, F. Sahin, R. Rao, and S. Brockport, "Darwinian particle swarm optimization," in *Proceedings of the 2nd Indian International Conference on Artificial Intelligence (IICAI '05)*, pp. 1474–1487, December 2005.
- [39] M. S. Couceiro, N. M. F. Ferreira, and J. A. T. Machado, "Fractional order Darwinian particle swarm optimization," in *Proceedings of the Symposium on Fractional Signals and Systems (FSS '11)*, Coimbra, Portugal, 2011.
- [40] M. Mashor, "Hybrid training algorithm for RBF network," *International Journal of the Computer, the Internet and Management*, vol. 8, pp. 50–65, 2000.
- [41] N. A. M. Isa, S. A. Salamah, and U. K. Ngah, "Adaptive fuzzy moving K-means clustering algorithm for image segmentation," *IEEE Transactions on Consumer Electronics*, vol. 55, no. 4, pp. 2145–2153, 2010.
- [42] W. Cai, S. Chen, and D. Zhang, "Fast and robust fuzzy c-means clustering algorithms incorporating local information for image segmentation," *Pattern Recognition*, vol. 40, no. 3, pp. 825–838, 2007.
- [43] S. Das, A. Abraham, and A. Konar, "Spatial information based image segmentation using a modified particle swarm optimization algorithm," in *Proceedings of the 6th IEEE International Conference on Intelligent Systems Design and Applications (ISDA '06)*, pp. 438–444, October 2006.
- [44] M. M. Trivedi and J. C. Bezdek, "Low-level segmentation of aerial images with fuzzy clustering," *IEEE Transactions on Systems, Man and Cybernetics*, vol. 16, no. 4, pp. 589–598, 1986.
- [45] F. U. Siddiqui and N. A. Mat Isa, "Enhanced moving K-means (EMKM) algorithm for image segmentation," *IEEE Transactions on Consumer Electronics*, vol. 57, no. 2, pp. 833–841, 2011.
- [46] L. P. Maguluri, K. Rajapanthula, and N. S. Parvathaneni, "A comparative analysis of clustering based segmentation algorithms in microarray images," *International Journal of Emerging Science and Engineering*, vol. 1, no. 5, pp. 27–32, 2013.
- [47] S. Ghosh and S. K. Dubey, "Comparative analysis of k-means and fuzzy c-means algorithms," *International Journal of Advanced Computer Science and Applications*, vol. 4, no. 4, 2013.
- [48] D. Martin, C. Fowlkes, D. Tal, and J. Malik, "A database of human segmented natural images and its application to evaluating segmentation algorithms and measuring ecological statistics," in *Proceedings of the 8th IEEE International Conference on Computer Vision (ICCV '01)*, vol. 2, pp. 416–423, 2001.
- [49] P. Jaccard, "The distribution of the flora in the alpine zone," *New Phytologist*, vol. 11, no. 2, pp. 37–50, 1912.
- [50] Z. Wang, A. C. Bovik, H. R. Sheikh, and E. P. Simoncelli, "Image quality assessment: from error visibility to structural similarity," *IEEE Transactions on Image Processing*, vol. 13, no. 4, pp. 600–612, 2004.



Hindawi

Submit your manuscripts at
<http://www.hindawi.com>

